IEEE Access
Multidisciplinary | Rapid Review | Open Access Journal

Received January 26, 2020, accepted March 1, 2020, date of publication March 17, 2020, date of current version March 26, 2020.

Digital Object Identifier 10.1109/ACCESS.2020.2981492

Combining Spectral and Texture Features for Estimating Leaf Area Index and Biomass of Maize Using Sentinel-1/2, and Landsat-8 Data

PEILEI LUO[1,2], JINGJUAN LIAO[1], AND GUOZHUANG SHEN[1]
[1]Key Laboratory of Digital Earth Science, Aerospace Information Research Institute, Chinese Academy of Sciences, Beijing 100094, China
[2]College of Resources and Environment, University of Chinese Academy of Sciences, Beijing 100094, China

Corresponding author: Jingjuan Liao (liaojj@radi.ac.cn)

This work was supported by the National Key Research and Development Program of China under Grant 2016YFB0501501.

ABSTRACT Leaf area index (LAI) and biomass are important indicators that reflect the growth status of maize. The optical vegetation indices and the synthetic-aperture radar (SAR) backscattering coefficient are commonly used to estimate the LAI and biomass. However, previous studies have suggested that spectral features extracted from a single pixel have a poor ability to describe the canopy structure. In this paper, we propose a method for estimating LAI and biomass by combining spectral and texture features. Specifically, LAI, biomass and remote-sensing data were collected from the jointing, trumpet, flowering, and filling stages of maize. Then we formed six remote-sensing feature matrices using the spectral and texture features extracted from the remote sensing data. Principal component analysis (PCA) was used to remove noise and to reduce and integrate the multi-dimensional features. Multiple linear regression (MLR) and support vector regression (SVR) methods were used to build the estimation models. Tenfold cross-validation was adopted to verify the effectiveness of the proposed method. The experimental results show that using the texture features of both optical and SAR data improves the estimation accuracy of LAI and biomass. In particular, SAR texture features greatly improve the estimation accuracy of biomass. The estimation model constructed by combining spectral and texture features of optical and SAR data achieves the best performance (highest coefficient of determination (R^2) and lowest root mean square error (RMSE)). Specifically, we conclude that the best window sizes for extracting texture features from optical and SAR data are 3×3 and 7×7, respectively. SVR is more suitable for estimating the LAI and biomass of maize than MLR. In addition, after adding texture features, we observed a significant improvement in the accuracy of estimation of LAI and biomass for the growth stages, which have a larger variation in the extent of the canopy. Overall, this work shows the potential of combining spectral and texture features for improving the estimation accuracy of LAI and biomass in maize.

INDEX TERMS Maize LAI and biomass, sentinel-1/2, spectral features, SVR, texture features.

I. INTRODUCTION

The leaf area index (LAI) and biomass are important indicators for monitoring the growth of maize [1]–[3]. They provide important information for monitoring temperature stress, water stress, pest levels, early yields, etc. [4]–[12]. Traditional LAI and biomass measurements rely on destructive sampling and manual measurements, which are time-consuming and labor-intensive [13]. The remote-sensing inversion method reduces the amount of time and labor needed to obtain LAI and biomass [14], [15], and it is widely used to measure growth metrics for crops such as maize [14]–[16], wheat [17], [18], rice [19]–[21], and soybean [22], [23]. With the rapid development of remote-sensing technology, the inversion of LAI and biomass from remote-sensing images has become a hot topic.

Spectral reflectance and vegetation indices extracted from optical data and the backscattering coefficient and polarization metrics extracted from synthetic-aperture radar (SAR) data are widely used for estimating LAI and biomass [23]–[27]. However, when the density of canopy leaves is high, the spectral reflectance and vegetation indices of optical data tend to be saturated. For example, the normalized difference vegetation index (NDVI), the most commonly used

The associate editor coordinating the review of this manuscript and approving it for publication was Pia Addabbo.

vegetation index, is sensitive for lower LAI values (<3), but is saturated for medium or higher LAI values (>3) [23]–[26]. Similarly, when the biomass is at a medium to high level (>2 kg m^{-2}), NDVI also tends to be saturated [23], [27]. Since SAR has good penetrability, the backscattering coefficient and polarization metrics extracted from SAR data can mitigate the saturation in estimating LAI and biomass [18], [28]. Conversely, SAR data are easily affected by the soil background and terrain factors. Recent studies have demonstrated that SAR data are still unable to obtain good estimates for LAI and biomass [13]. Obviously, it is difficult to describe accurately the complex canopy structure based on the optical and SAR remote-sensing features extracted from single pixels [29]. Therefore, the influence of surrounding pixels on the target pixels should be considered when estimating LAI and biomass [30], [31].

However, texture features can describe the spatial correlation of pixels, and help to reflect the variation of vegetation structure [32]. At present, texture features are widely used in classification research, indicating that texture features can help to improve classification accuracy [31], [33]. Kwak and Park used texture features extracted from a gray-level co-occurrence matrix (GLCM) along with spectral features to classify crops, which improved the classification accuracy by 7.72% [31]. Other researchers have suggested that spectral information alone is often insufficient for discriminating between the regeneration and successional stages of coniferous forest but textural information can be useful to distinguish the variation of the forest structure [33]. Some studies have demonstrated that texture features are useful for estimating LAI and biomass [29], [34]–[40]. Wulder *et al.* used texture features with a vegetation index to improve the inversion of LAI [29], especially when LAI > 3 [34]. Zhou *et al.* extracted texture features from QuickBird images to estimate LAI for a broad-leaved forest. They found that the accuracy of estimates of LAI are better when LAI > 3. The maximum R^2 in LAI estimation was obtained from the angle second-order moment (ASM) and entropy (ENT) extracted from a 3 × 3 moving window [35]. Yue *et al.* noted that when biomass is at a high level, the accuracy of biomass estimates can be improved by combining vegetation indices and texture features compared with using a vegetation index alone [36]. Ouma and Tateishi studied the inversion of forest biomass using texture features. Using a combination of texture features and a vegetation index gave the best results [37]. Moreover, the best extraction window size and texture features are related to the height, species, age, and spatial distribution of the vegetation canopy [37]. Overall, while texture features are useful for estimating LAI and biomass [37]–[40], few studies have examined the effect of texture features in estimating LAI and biomass in maize.

In addition, the response mechanisms of optical and SAR images to the vegetation canopy are different. Therefore, it is worth exploring whether a combination of optical and radar data can improve the accuracy of estimates of LAI and biomass. Previous studies have shown that a combination of SAR and multi-spectral data can improve the accuracy of estimates of LAI and biomass [18], [41]–[45]. Bach *et al.* noted that using a combination of RapidEye and TerraSAR-X images to extract LAI can mitigate the dependence on weather conditions [42]. Hosseini *et al.* concluded that comprehensively using optical and SAR images can overcome the loss of data caused when the details of an optical image are obscured by cloud [43]. Naidoo *et al.* suggested that integrating optical and SAR data can reduce the impact of soil background and weather conditions on estimates of biomass [44]. Gao *et al.* showed that a new vegetation index constructed by combining optical and SAR images has a good correlation with LAI and biomass in maize, and can improve the accuracy of inversion for LAI and biomass of maize [45]. However, there has been little research on the inversion of LAI and biomass by leveraging texture features from a combination of optical and SAR data.

Thus, in this paper, we combine texture and spectral features from optical and SAR data to estimate LAI and biomass. Our overall objectives are: (1) to study the effects of texture features from optical and SAR data and their combination on estimates of LAI and biomass in maize, (2) to investigate the effects of changes in the window size on the extraction of texture features when estimating LAI and biomass maize, and (3) to study the effect of texture features on the accuracy of estimates of LAI and biomass for maize at different growth stages.

II. MATERIALS

A. STUDY AREA

The study area is located in Wuqing District, Tianjin, China (Figure 1). It has a total area of 1574 km^2, of which 913 km^2 is arable land, accounting for 58% of the land area. This area is in the lower part of the North China Plain and has relatively flat terrain. There are mainly three soil types: sandy soil, loamy soil, and clayey soil. The soil is loose and fertile, making it suitable for the cultivation of crops. This area has a warm temperate semi-humid continental monsoon climate with four distinct seasons. The annual average temperature is 11.6°C, the average temperature in January is −5.1°C, the average temperature in July is 26.1°C, and the average annual amount of sunshine is 2705 hours. The annual average precipitation is 606.8 mm, and the annual average frost-free period is 212 days. The main crop planted in summer in this area is maize, accounting for 78.3% of the total, followed by soybeans, accounting for 8.9% of the total, and rice and grassland [46].

B. DATA

1) SATELLITE DATA COLLECTION AND PROCESSING

Data from three satellites (Sentinel-1, Sentinel-2, and Landsat-8) were acquired at the jointing stage, trumpet stage, flowering stage, and filling stage of maize in 2018 (Table 1). Four Sentinel-1 ground range detected (GRDH) images, four Sentinel-1 single look complex (SLC) images,

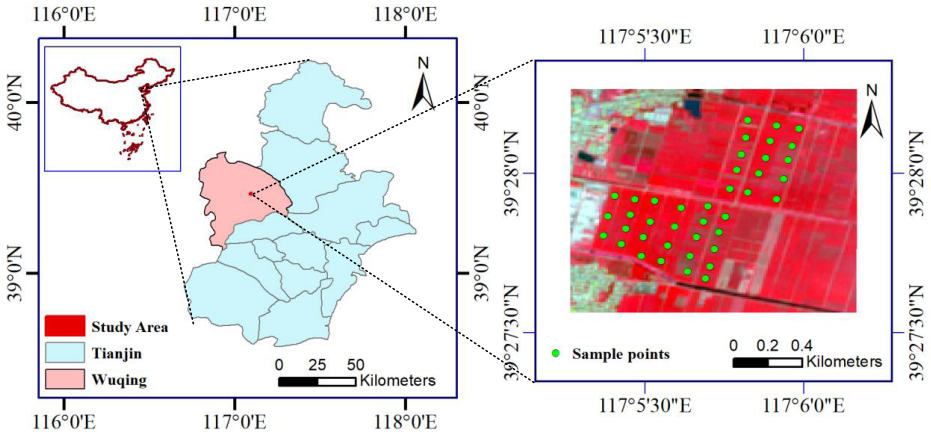

FIGURE 1. Location of the study area and the distribution of sample points.

TABLE 1. Satellite data sets.

Data set		Date of acquisition (month/day)	Resolution	Source	Frequency
SAR data	Sentinel-1B SLC	7/20, 8/1, 8/18, 8/30	5 × 20 m	ESA	12 days
	Sentinel-1B GRDH	7/20,8/1,8/18,8/30	22 × 20 m	ESA	12 days
Optical data	Sentinel-2A MSI	8/3, 8/16, 9/5	10 × 10 m	ESA	10 days
	Landsat-8 OLI	7/22	15 × 15 m	USGS	16 days

and three Sentinel-2 L1C multi-spectral images (MSI) were downloaded from ESA's scientific data interface (https://scihub.copernicus.eu/dhus/#/home), and one Landsat-8 OLI image was downloaded from USGS Earth Explorer (https://earthexplorer.usgs.gov/). The spatial resolutions of the SLC and GRDH data from Sentinel-1 were 5 × 20 (range [m] × azimuth [m]) and 20 × 22 (range [m] × azimuth [m]), respectively. The spatial resolution of the Sentinel-2 L1C multi-spectral data was 10 × 10 m. The spatial resolution of the Landsat-8 OLI data was 30 m in the multi-spectral band and 15 m in the panchromatic band. In the jointing period, the Sentinel-2 images had thick cloud cover, so Landsat-8 OLI data that had no clouds were used instead for the same stage.

The preprocessing of SLC and GRDH data was based on the SNAP software downloaded from the official ESA website. It mainly included radiometric calibration, multi-look processing, refined Lee filtering, and geocoding. The preprocessing of Sentinel-2 L1C multi-spectral data was carried out with the Sen2cor plug-in provided by ESA [47]. First, the L1C data underwent radiometric calibration and atmospheric correction to obtain L2 data, and then the bands 5, 6, 7, 8A, 11, and 12 were resampled to a spatial resolution of 10 × 10 m consistent with other bands. The software ENVI was used to preprocess the Landsat-8 OLI data. First, the spectrum and panchromatic band were fused to obtain multi-spectral data with a resolution of 15 m, then the radiometric calibration and atmospheric correction were performed. It should be noted that we have carried out geometric rectification for all the above data in the end.

2) IN-SITU LAI AND BIOMASS MEASUREMENTS

In-situ LAI and biomass (Table 2) of four growth stages (jointing, trumpet, flowering, and filling) were measured on July 20 to 23, July 31 to August 2, August 15 to 17, and September 3 to 5, 2018, respectively. Altogether, 40 sample points (Figure 1) were selected in the study area. Each sample point was selected in the center of a quadrat of 100 × 100 m based on the remote sensing image, and the location of each sample point was measured by Garmin GPS 60. For each sample point, we measured the plant parameters of maize, including leaf length, leaf width, biomass, and plant density. The dry biomass of maize was obtained by multiplying the dry weight of the plant by density, and the dry weight was measured by cutting the sample of maize and dried it in

TABLE 2. Measured LAI and biomass of maize in Wuqing area.

Growth stage	LAI			Biomass ($g\,m^{-2}$)		
	Min	Max	Mean	Min	Max	Mean
7/20–7/23 (Jointing)	0.38	2.34	1.23	16.48	190.14	84.46
7/31–8/2 (Trumpet)	1.37	4.58	2.88	93.60	697.78	307.55
8/15–8/17 (Heading)	2.20	4.84	3.49	242.68	963.31	628.28
9/3–9/5 (Filling)	1.55	5.13	3.28	497.97	1559.08	1051.33

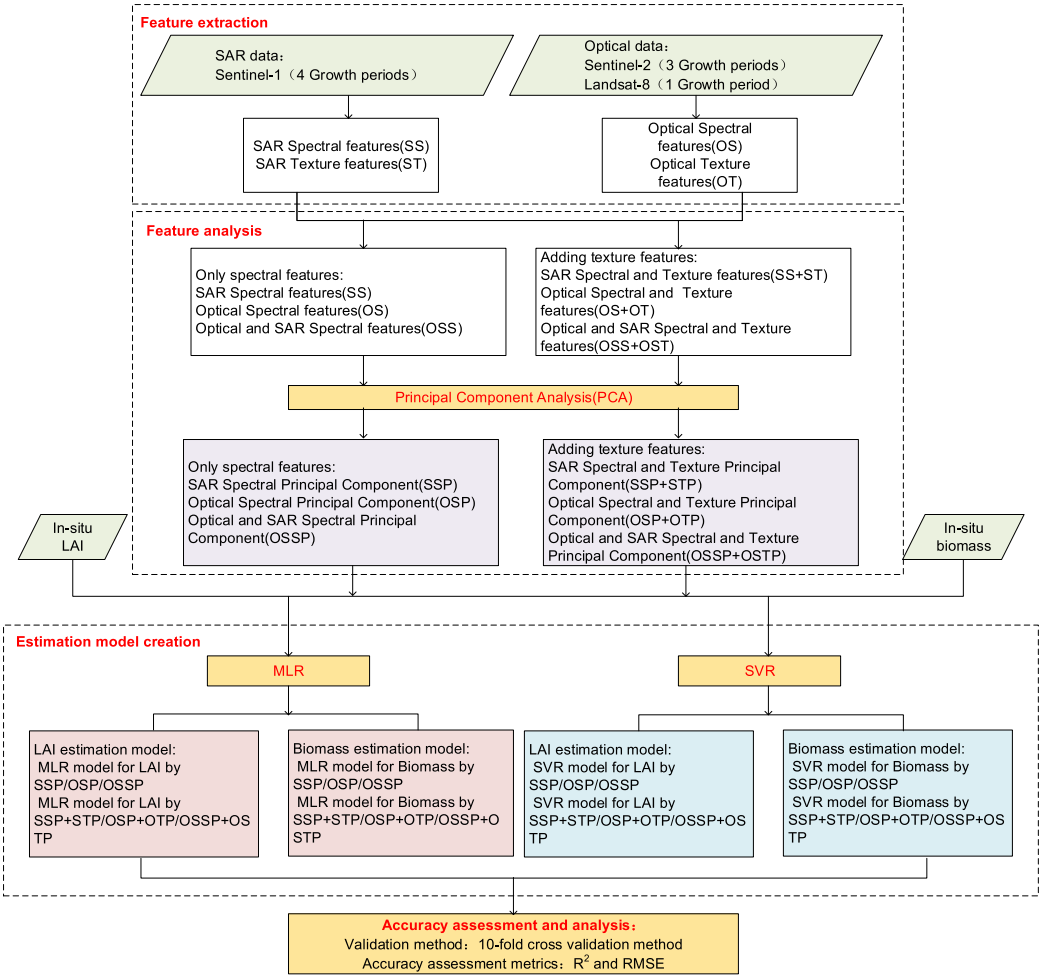

FIGURE 2. Flowchart for combining spectral and texture features in estimating maize LAI and biomass based on SAR and optical data.

an oven. Similarly, LAI was obtained by multiplying the area of single plant by plant density, where the area of single plant was calculated by sum all single leaf area of plant. The single leaf area of a plant can be calculated by multiplying leaf length by leaf width by 0.73. To ensure the accuracy of these parameters, in each quadrat we measured three representative samples and averaged the three samples (Table 2). For all in-situ samples, the range for LAI was 0.38–5.13, and the range for biomass was 16.48 g m^{-2}–1559.08 g m^{-2}.

III. METHODS

In this paper, we explore a method to leverage the spectral and texture features of optical and SAR data for estimating LAI and biomass in maize. The motivation is that, as we discussed in the introduction, (1) texture features can alleviate the saturation of spectral features in estimating LAI and biomass and (2) SAR has strong penetration and so can provide information that is complementary to optical data. Thus, this combination can yield more accurate estimates of LAI and biomass.

We propose a pipeline (Figure 2) that combines spectral and texture features from optical and SAR data for estimating LAI and biomass in maize. Specifically, we first extract abundant texture and spectral features from optical and SAR data. Then, PCA is leveraged to combine the extracted features and reduce the noise. Next, inversion models for LAI and biomass can be constructed based on MLR and SVR, respectively.

A. FEATURE EXTRACTION AND ANALYSIS

1) TEXTURE FEATURE EXTRACTION

The texture features of remote-sensing images can provide information about changes in the structure and geometric characteristics of ground objects [48], [49]. The most commonly used method to extract texture features is statistical analysis. In this paper, it was used to extract eight texture features from the GLCM of optical and SAR images [50]: mean (MEA), variance (VAR), homogeneity (HOM), contrast (CON), dissimilarity (DIS), entropy (ENT), angular second moment (ASM), and correlation (COR). Then, we extracted the texture features of the 40 sample points according to the geographic coordinates recorded with a Garmin GPS 60.

TABLE 3. Texture features.

Data set		Image bands	Window sizes	Matrices
SAR	Sentinel-1B GRDH	$\sigma^0_{VV}, \sigma^0_{VH}, \sigma^0_{VV/VH}$	$3\times3, 5\times5, 7\times7$	ST, OST
Optical	Sentinel-2A MSI	B2–B4, B8, B11–B12	$3\times3, 5\times5, 7\times7$	OT, OST
	Landsat-8 OLI	B2–B8	$3\times3, 5\times5, 7\times7$	OT, OST

In addition, the image texture measures the local variance of gray level, which is largely dependent on the scale [51]. Therefore, when extracting texture features, we need to select the appropriate window size. In this paper, we compared 3×3, 5×5, and 7×7 windows when extracting texture features from optical and SAR data to find the best size for estimating LAI and biomass for maize (Table 3).

2) SPECTRAL FEATURE EXTRACTION

Spectral features, such as spectral reflectance and vegetation indices, are often used to estimate the LAI and biomass of crops [23]–[26]. In addition, the backscattering coefficient and polarization metrics extracted from SAR images are also often used to retrieve the LAI and biomass of crops [52]. Many studies have shown that these features extracted from optical and SAR images have a good correlation with LAI and biomass [18], [45]. Therefore, the spectral reflectance of six bands of optical data (blue, green, red, near infrared, short infrared 1, and short infrared 2), five vegetation indices [NDVI [53], enhanced vegetation index (EVI) [54], ratio vegetation index (RVI) [55], soil-adjusted vegetation index (SAVI) [56], and modified soil-adjusted vegetation index (MSAVI) [57]] and the backscattering coefficient and polarization metrics (H, A, and α) from SAR data were extracted (Table 4). For simplicity, the above features (spectral reflectance, vegetation indices, backscattering coefficient, and polarization metrics), which are based on single-pixel extraction, are collectively referred to as spectral features in this paper. Similarly, we extracted spectral features for the 40 sample points according to the geographic coordinates recorded with the Garmin GPS 60.

For these features extracted from optical and SAR remote-sensing images, six feature matrices were created: optical spectral feature matrix (OS), optical texture feature matrix (OT), SAR spectral feature matrix (SS), SAR texture feature matrix (ST), optical + SAR spectral feature matrix (OSS), and optical + SAR texture feature matrix (OST).

3) FEATURE ANALYSIS

PCA can compress multi-dimensional variables into fewer variables in a principal component vector while retaining the main parts of the information in the original data. PCA is widely used in remote-sensing data decorrelation and noise processing [58], [59]. Fei *et al.* noted that compared with look-up table methods and artificial neural networks, PCA can give better results for estimating the LAI of maize [60]. The extracted texture and spectral features contain rich ground feature information, but there may be correlations between the features. Therefore, PCA is used to reduce the dimensionality and denoise the multi-dimensional feature matrix. In this paper, the PCA of the feature matrices (OS, OS + OT, SS, SS + ST, OSS, and OSS + OST) is implemented in Python to give the new remote-sensing feature matrices (OSP, OSP + OTP, SSP, SSP + STP, OSSP, and OSSP + OSTP), which are composed of the principal components.

B. MODEL BUILDING METHODS

To express quantitatively the relation between multi-dimensional remote-sensing features and maize LAI and biomass, this paper takes the multi-dimensional remote-sensing features as independent variables, the in-situ LAI and biomass of maize as dependent variables, and establishes an MLR model and an SVR model, respectively [39], [61]. The MLR model and the SVR model express the linear and nonlinear relations between remote-sensing features and the LAI and biomass of maize.

The MLR model uses the least squares method for the regression analysis:

$$\text{LAI} = a_0 + a_1x_1 + a_2x_2 + \cdots + a_nx_n \quad (1)$$

$$\text{Biomass} = b_0 + b_1x_1 + b_2x_2 + \cdots + b_nx_n \quad (2)$$

where $x_1, x_2, \ldots, x_n$ are the multi-dimensional remote-sensing features and $a_0, a_1, a_2, \ldots, a_n$ and $b_0, b_1, b_2, \ldots, b_n$ are the regression coefficients for the MLR model. n is the number of independent variables.

The SVR model uses the Lagrange multiplier method for the regression analysis:

$$\text{LAI} = \omega_1\phi_1(x) + b_1 \quad (3)$$

$$\text{Biomass} = \omega_2\phi_2(x) + b_2 \quad (4)$$

where x is the multi-dimensional remote-sensing feature, $\phi_1(x)$ and $\phi_2(x)$ are the kernel functions, and ω_1, b_1, ω_2, and b_1 are the parameters to be found. Here, for the kernel function we use a Gauss function as the radial basis function.

In addition, to explore the influence of texture features on the LAI and biomass estimation models, the main components without texture features, such as OSP, SSP, and OSSP and with texture features, such as OSP + OTP, SSP + STP, and OSSP + OSTP are used as the inputs of the two estimation models, respectively. The models for maize LAI and biomass are then constructed using MLR and SVR.

TABLE 4. Spectral features.

Data set		Spectral features	Matrices
SAR	Sentinel-1B SLC	H, A, α	SS, OSS
	Sentinel-1B GRDH	σ^0_{VV}, σ^0_{VH}, $\sigma^0_{VV/VH}$	SS, OSS
Optical	Sentinel-2A MSI	B2–B4, B8, B11–B12, NDVI, RVI, EVI, SAVI, MSAVI	OS, OSS
	Landsat-8 OLI	B2–B8, NDVI, RVI, EVI, SAVI, MSAVI	OS, OSS

TABLE 5. Accuracy of LAI and biomass estimation models for maize using only SAR or only optical data.

Feature matrices	LAI				Biomass			
	R^2		RMSE		R^2		RMSE ($g\,m^{-2}$)	
	MLR	SVR	MLR	SVR	MLR	SVR	MLR	SVR
OSP	0.488	0.598	0.657	0.665	0.387	0.535	272.171	255.518
OSP + OTP (3×3)	0.587	0.645	0.575	0.632	0.561	0.679	219.017	207.653
OSP + OTP (5×5)	0.582	0.612	0.583	0.660	0.523	0.677	232.940	208.479
OSP + OTP (7×7)	0.537	0.621	0.622	0.660	0.478	0.670	243.519	220.318
SSP	0.100	0.104	0.887	0.909	0.203	0.201	301.888	308.991
SSP + STP (3×3)	0.250	0.376	0.770	0.753	0.521	0.534	220.729	229.250
SSP + STP (5×5)	0.252	0.378	0.767	0.753	0.538	0.569	213.465	217.206
SSP + STP (7×7)	0.254	0.384	0.766	0.748	0.555	0.583	206.145	212.845

TABLE 6. Accuracy of LAI and biomass estimation models for maize using both SAR and optical data.

Feature matrices	LAI				Biomass			
	R^2		RMSE		R^2		RMSE ($g\,m^{-2}$)	
	MLR	SVR	MLR	SVR	MLR	SVR	MLR	SVR
OSSP	0.525	0.621	0.630	0.681	0.432	0.597	243.503	248.141
OSSP + OSTP (3×3)	0.611	0.671	0.563	0.640	0.577	0.682	202.529	208.996
OSSP + OSTP (5×5)	0.607	0.672	0.568	0.634	0.548	0.707	211.877	202.854
OSSP + OSTP (7×7)	0.579	0.641	0.593	0.662	0.554	0.699	210.606	213.028

C. ACCURACY

Tenfold cross-validation was used to assess the accuracy of the various LAI and biomass estimation models based on different remote-sensing features and different methods [62]. First, the data set was randomly divided into 10 parts. Nine of them were used as training data and one was used as test data in training the model [40], [62]. The R^2 and the root-mean-square error (RMSE) were used to assess the precision of the LAI and biomass estimation models:

$$R^2 = \frac{\sum_{i=1}^{n}(f_i - \bar{y})^2}{\sum_{i=1}^{n}(y_i - \bar{y})^2} \tag{5}$$

$$\text{and RMSE} = \sqrt{\frac{\sum_{i=1}^{n}(f_i - y_i)^2}{n}}, \tag{6}$$

where f_i denotes the simulated value of LAI or the biomass obtained from the estimation model, and y_i and $\bar{y}_i$ denote the in-situ value and mean value, respectively. n denotes the number of sample points ($n = 1, 2, 3, \ldots$). Each model was tested 10 times, and the mean value of the 10 runs was taken as the final result.

IV. RESULTS

A. ESTIMATION OF MAIZE LAI AND BIOMASS USING SPECTRAL AND TEXTURE FEATURES

Figures 3 and 4 compare the predicted and measured values for the inversion model. It can be seen from the two figures that the estimation model constructed from optical + SAR data has the highest R^2 (MLR: LAI $R^2 = 0.610$, biomass $R^2 = 0.577$; SVR: LAI $R^2 = 0.672$, biomass $R^2 = 0.707$) and the lowest RMSE (MLR: LAI RMSE = 0.563, biomass RMSE = 202.529 $g\,m^{-2}$; SVR: LAI RMSE = 0.634, biomass RMSE = 202.854 $g\,m^{-2}$). The SVR model is better for estimating LAI and biomass than the MLR model. However, the LAI model constructed by SAR data is not good, while the biomass model constructed by SAR data is good. Tables 5 and 6 show the accuracy of the estimation

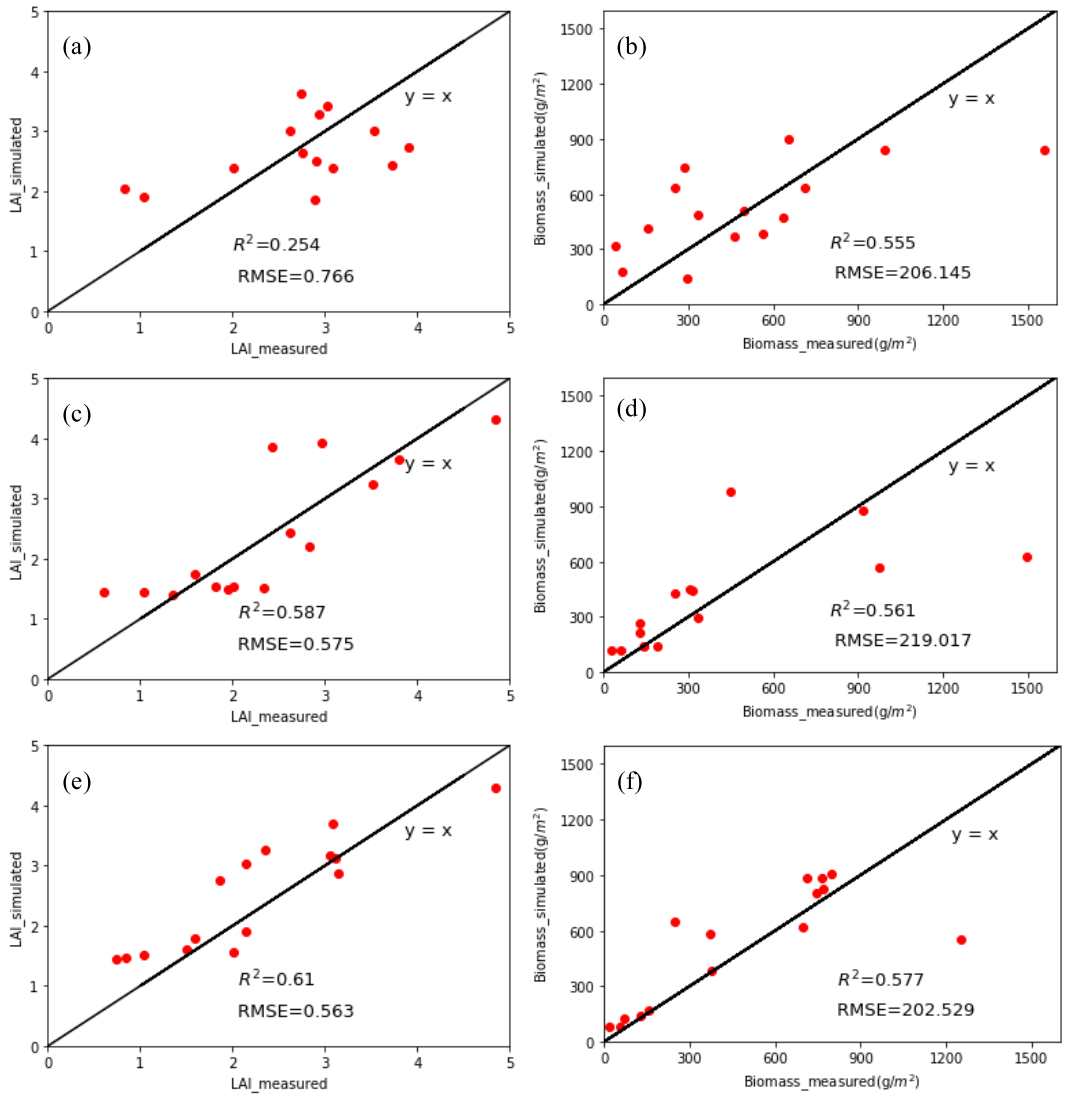

FIGURE 3. Comparison of measured values of LAI and biomass with values from estimation models based on MLR: (a) LAI model using SAR data, (b) biomass model using SAR data, (c) LAI model using optical data, (d) biomass model using optical data, (e) LAI model using both SAR and optical data, and (f) biomass model using both SAR and optical data.

models. As can be seen, when texture features are added, the R^2 values of LAI and biomass are higher and the RMSE values are lower.

B. ESTIMATION OF MAIZE LAI AND BIOMASS AT DIFFERENT GROWTH STAGES

The effect of texture features on estimates of maize LAI and biomass at different growth stages can be seen in Figure 5. For the MLR method, R^2 decreased at the trumpet stage, whereas it increased at this stage with the SVR method. This shows that nonlinear models are better than linear models in estimating this vigorous growth stage of maize. R^2 is a maximum at the peak of maize growth (heading or flowering stage). R^2 is the lowest for the models without texture features as OSSP, and increased by 0.1–0.3 when texture features were added, which indicates that texture features are important in compensating for saturation.

V. DISCUSSION

A. THE EFFECT OF USING ONLY OPTICAL OR ONLY SAR TEXTURE INFORMATION ON LAI AND BIOMASS ESTIMATES

To explore the effects of incorporating texture information on maize LAI and biomass estimates, spectral and texture features extracted from optical and SAR data were used to build MLR and SVR models, respectively. The results show that models built by combining spectral and texture features performed better than models based on spectral features alone (Figure 6). These results are in agreement with the wheat biomass estimates made by Zhou *et al.* [35], the wheat LAI estimates made by Li *et al.* [63], and the forest biomass estimates made by Cutler *et al.* [49].

Figures 6(a) and 6(b) show the R^2 of LAI and biomass models built by MLR and SVR, respectively, whereas Figures 6(c) and 6(d) show the RMSE values. The texture

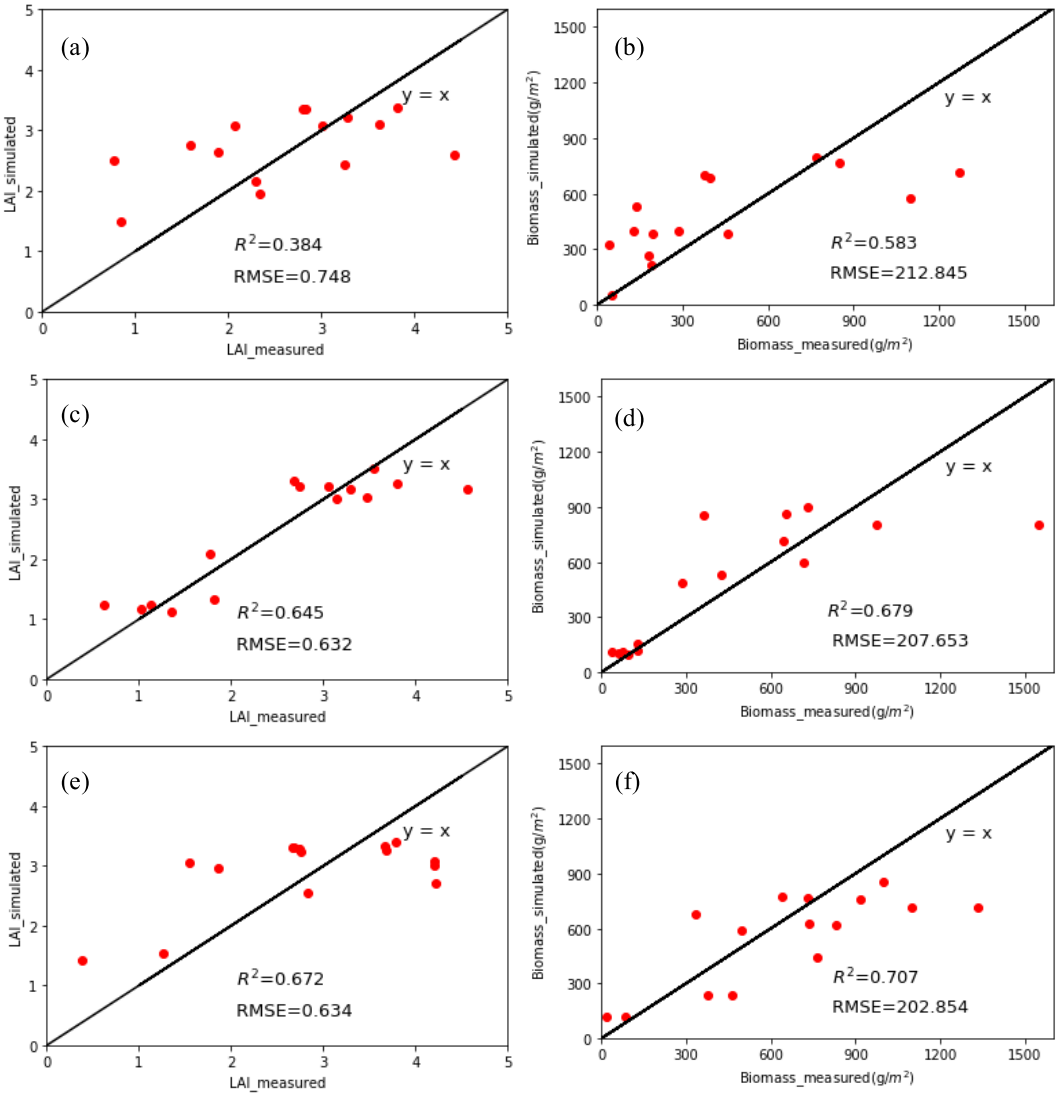

FIGURE 4. Comparison of measured values of LAI and biomass with values from estimation models based on SVR: (a) LAI model using SAR data, (b) biomass model using SAR data, (c) LAI model using optical data, (d) biomass model using optical data, (e) LAI model using both SAR and optical data, and (f) biomass model using both SAR and optical data.

features extracted from SAR data have a more significant effect than optical texture features, especially for estimating biomass. After adding SAR texture information, the R^2 of the biomass models increased by about 0.35, and that of the LAI models increased by about 0.15. However, with the addition of optical texture features, the R^2 of the LAI and biomass models increased only by about 0.1. This may mean that the SAR texture features provide more information about the maize canopy, which is useful in estimating LAI and biomass. Moreover, due to the side-looking imaging of SAR, its texture information may better describe the structural characteristics of the canopy, which is a good supplement to the spectral characteristics. In conclusion, both optical and SAR texture information can improve the accuracy of estimates of maize LAI and biomass. SAR texture information, in particular, is most beneficial to estimates of biomass.

B. COMPARISON OF LAI AND BIOMASS ESTIMATES MADE BY COMBINING OPTICAL AND SAR DATA WITH ESTIMATES MADE USING ONLY OPTICAL OR ONLY SAR DATA

Due to the different imaging techniques used for optical and SAR data, the remote-sensing information they contain is quite different. Therefore, the influence of combining optical and SAR data on the construction of maize LAI and biomass estimation models was analyzed. Figure 7 illustrates that combining optical and SAR features improves the accuracy of LAI and biomass estimates. Moreover, the models have the highest accuracy after adding texture features. For both MLR and SVR models, R^2 is higher and RMSE is somewhat lower after combining optical and SAR features. Therefore, the combination of optical and SAR remote-sensing data can provide more information for LAI and biomass estimation models, which is consistent with the results of

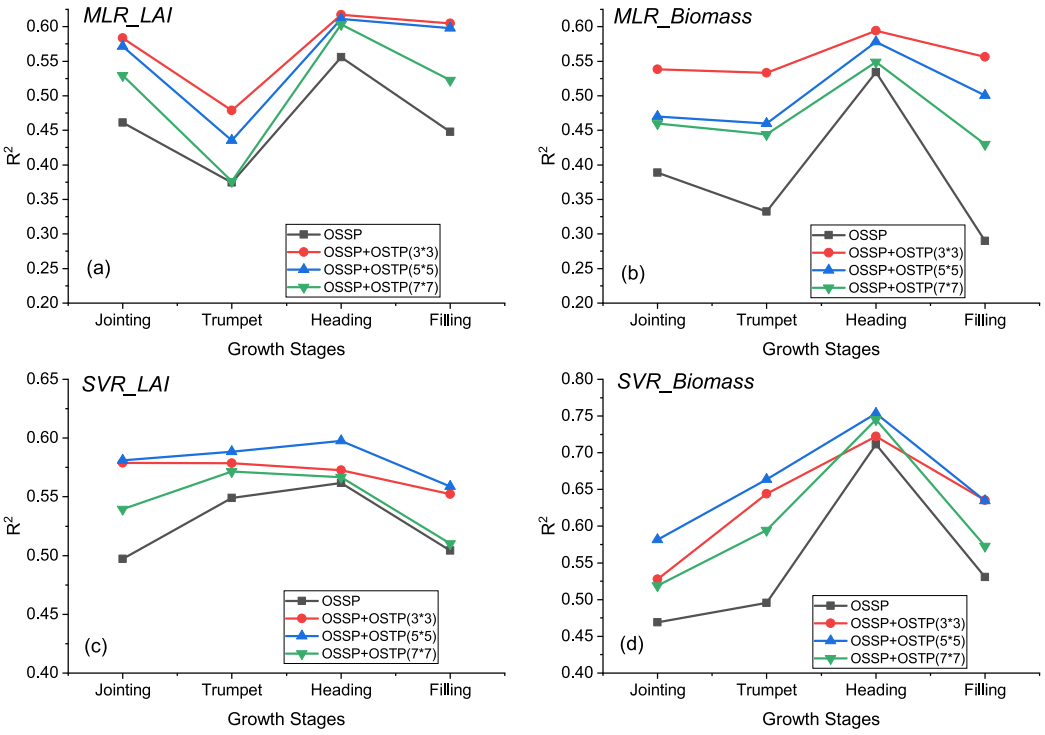

FIGURE 5. Comparison of LAI and biomass estimation models at different growth stages. OSSP indicates that spectral features were extracted from a combination of optical and SAR data, whereas OSSP + OSTP indicates that spectral features and texture features were extracted from a combination of optical and SAR data. The sizes of the windows for extracting texture features were 3 × 3, 5 × 5, and 7 × 7.

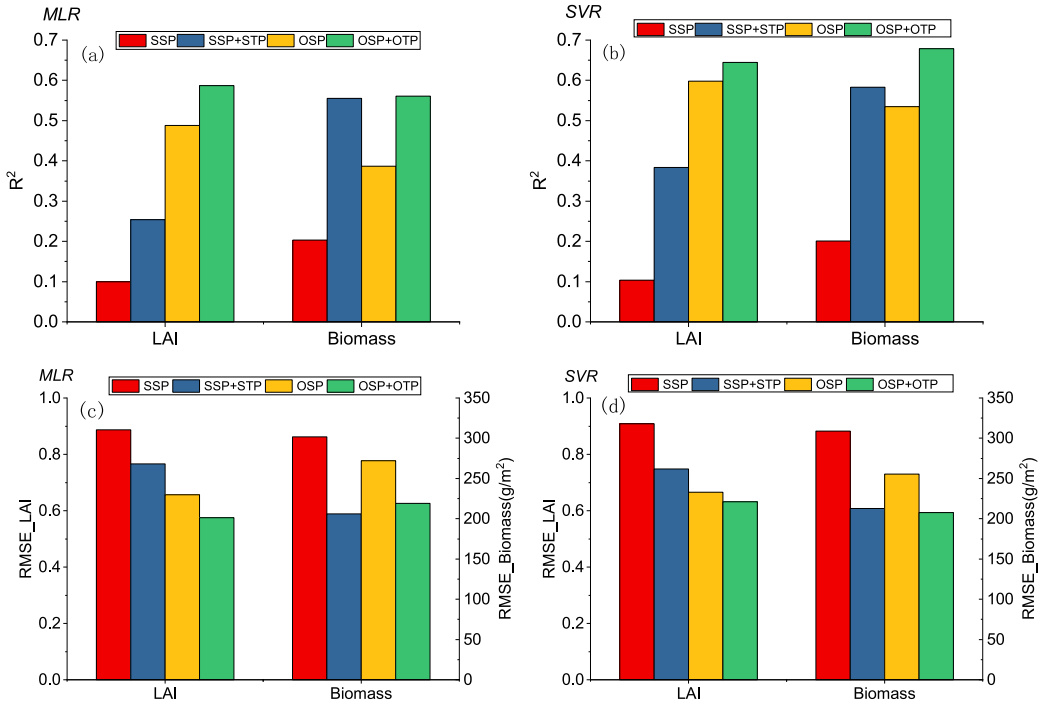

FIGURE 6. Contributions of texture features extracted from only optical or only SAR data to LAI and biomass estimates. (a), (b) R^2 for LAI and biomass models based on MLR or SVR, respectively. (c), (d) RMSE for LAI and biomass models based on MLR or SVR, respectively.

Zhou *et al.* [35] and Yue *et al.* [36]. This may be due to the different response mechanism of the optical data and SAR data for ground objects. Optical data may have a rich amount of spectral information in the visible band, but can not reflect the contribution of the inner leaves of the canopy. In contrast, SAR has good penetrability, and the side-looking imaging

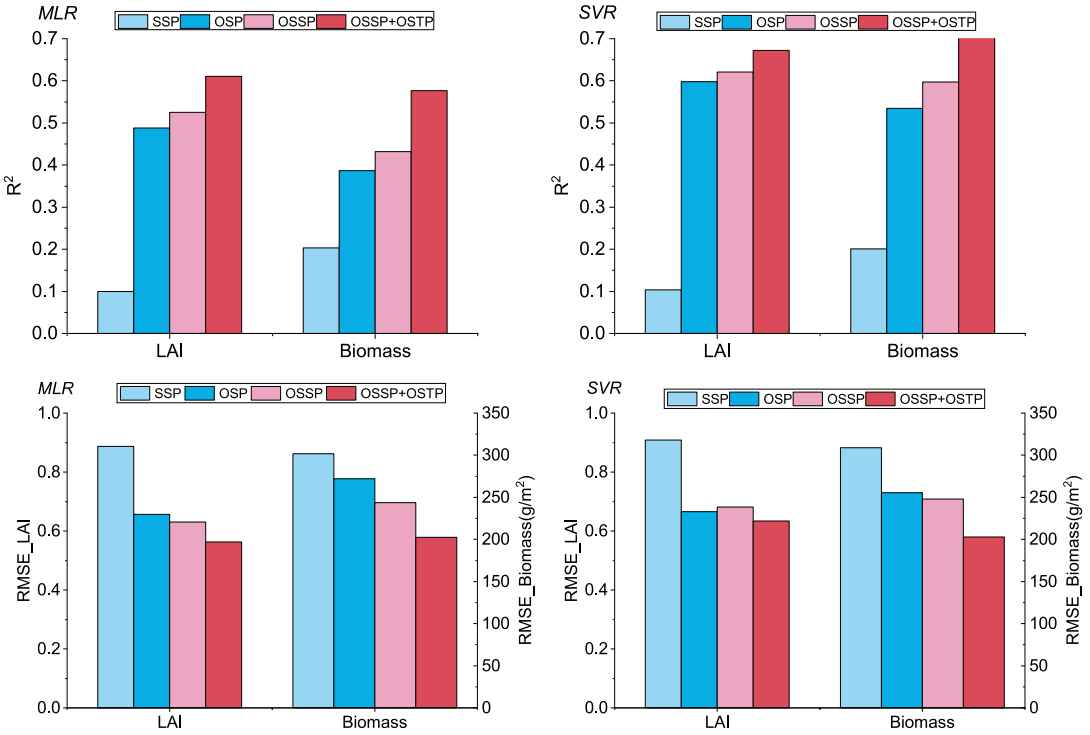

FIGURE 7. Comparisons of combining optical and SAR data with only optical or only SAR data in LAI and biomass estimation. (a), (b) R^2 of LAI and biomass models based on MLR or SVR, respectively. (c), (d) RMSE of LAI and biomass models based on MLR or SVR, respectively.

mode is helpful for obtaining more information about the canopy structure, which can compensate for the deficiencies of optical data. Therefore, the combination of the two can complement each other to get better inversion results.

C. SENSITIVITY OF FEATURE EXTRACTION WINDOW SIZE IN LAI AND BIOMASS ESTIMATION MODELS

In this paper, the texture features of optical and SAR data were extracted with windows of size 3 × 3, 5 × 5, and 7 × 7, and the estimation models for maize LAI and biomass were constructed by combining spectral and texture features in different windows (Table 5). The experimental results show that the estimation models of LAI and biomass have the highest accuracy when the optical texture feature window is 3 × 3 and the SAR texture feature window is 7 × 7. As the feature extraction window increases in size (from 3 × 3 to 5 × 5 and 7 × 7), the accuracy of the models constructed with optical texture features gradually decreases. This may be because the differences between pixels are smoothed out by the window, resulting in a reduction of detail for the maize canopy. However, the models based on 7 × 7 texture features have the highest accuracy. It is possible that the SAR data include a significant amount of noise due to its special imaging mechanism, and the noise interferes with information extraction and analysis. With an increase of the window size, the noise becomes smoother, so a larger window may provide more effective information on the structure of the maize canopy. In addition, Table 6 and Figure 5 show that when combining optical and SAR data to estimate LAI and biomass, the optimal extraction window for texture features differs for the MLR and SVR models (3 × 3 and 5 × 5, respectively). Thus, the size of the extraction window for texture features affects the accuracy of estimates of LAI and biomass. Moreover, the sensitivity of the extraction window is also related to how the model is built and the type of remote-sensing data used. Therefore, the sensitivity of the texture feature extraction window needs to be analyzed under different conditions.

D. INFLUENCE OF LINEAR AND NONLINEAR INVERSION METHODS ON LAI AND BIOMASS ESTIMATION MODELS

In addition to the factors discussed above, whether a linear method as MLR or a nonlinear method as SVR is used also affects the accuracy of LAI and biomass estimation. As can be seen from Tables 5 and 6, whether the inversion model is constructed using only spectral features or using both spectral and texture features, the R^2 obtained by the SVR method is higher than that obtained by the MLR method, while RMSE is reduced by varying degrees. This indicates that the inversion model constructed by the SVR method is more accurate than that constructed by the MLR method, which is consistent with the results of Fei *et al.* [60]. This may be because MLR is suitable for estimating only remote-sensing features with a linear relation with LAI and biomass, whereas the relation between multi-dimensional remote-sensing features and LAI (or biomass) is not a simple linear correlation.

However, the nonlinear relation between multi-dimensional remote-sensing features and LAI (or biomass) is fully considered in the SVR method by using a radial basis function as the kernel function. Therefore, the precision of the LAI and biomass estimation model constructed by the SVR method was higher than that constructed by the MLR method. However, the LAI and biomass estimation models constructed by the MLR and SVR methods may be unstable when applied at a larger scale, since the parameters have regional applicability.

E. EFFECTS OF TEXTURE INFORMATION ON LAI AND BIOMASS ESTIMATION FOR DIFFERENT GROWTH STAGES OF MAIZE

Figure 6 shows that there is a significant regularity in the accuracy of LAI and biomass estimation models in the four growth stages. As mentioned above, the accuracy of LAI and biomass for models built by both the MLR and the SVR methods is the highest in the flowering stage. Because the growth and development of a maize canopy reaches a peak at the flowering stage, LAI and biomass no longer continue to grow rapidly. In addition, in the flowering stage, the bottom leaves have not started to fall off, so the canopy structure is relatively stable. The canopy closes over at the flowering stage, and the influence of the soil background on the optical and SAR features is weakened, so the accuracy of LAI and biomass estimation will be better. However, we found that the accuracy of estimates of LAI and biomass of maize at the flowering stage was not improved significantly by adding texture features, which indicates that the improvement from adding texture features on the accuracy of canopy growth parameters is smaller when the canopy structure is relatively stable. In contrast, adding texture features significantly enhances the accuracy of estimates of LAI and biomass in the jointing stage, the trumpet stage, and the filling stage. This is because when the canopy structure is changing rapidly, texture features are helpful in describing the changes in canopy growth parameters. The accuracy of biomass inversion in the trumpet stage is the highest with texture features, which is when the largest change occurs in the canopy structure. In conclusion, texture features are very sensitive to changes in the canopy structure and have great potential for estimating maize LAI and biomass, especially in the rapid growth stage.

VI. CONCLUSION

In this study, the method for estimating maize LAI and biomass by combining spectral and texture features was proposed through exploring various effects on estimation of maize LAI and biomass, including different satellite data, window sizes of feature extraction, modeling methods and growth stages. We used the optical and SAR data to extract the spectral and texture features. The spectral features include reflectance and vegetation indices extracted from optical data, and the backscattering coefficient and polarization metrics extracted from SAR data. The texture features include eight kinds of GLCM-based variables extracted from multiple optical and SAR data. In order to reduce the dimensionality and noise from these multi-dimensional features, PCA method was used to filter the unnecessary information and select the effective features, and MLR and SVR methods were used to build estimation models of maize LAI and biomass.

Based on this study, a combination of optical and SAR data can obtain better results than only using optical or SAR data, and SVR method is more suitable for estimating maize LAI and biomass than MLR method. The texture features extracted from the optical and SAR data can improve the estimation accuracy of maize LAI and biomass, and SAR texture features significantly improved the accuracy of biomass estimation. The window size of texture feature extraction has obvious influence on the accuracy of maize LAI and biomass estimates, and the optimal window size depends on the type of remote sensing data and the estimation method. Moreover, the texture features have different effects on maize LAI and biomass estimates at different growth stages, in particular, when the canopy structure of maize grows rapidly, such as the trumpet stage, the texture features have significant influence on maize LAI and biomass estimates, otherwise they have less influence when the growth is relatively stable, such as the flowering stage.

This study provides insights into combining spectral and texture features for estimating maize LAI and biomass using optical and SAR data. But this method is empirical, so its application is limited by in-situ data. Further evaluation of combining spectral and texture features for estimating the parameters of different crops need to be carried out in future research.

ACKNOWLEDGMENT

The authors would like to thank ESA and USGS for providing Sentinel-1, Sentinel-2, and Landsat-8 data. They would also like to thank their colleagues who participated in the field surveys and data collection and the editor and reviewers for their valuable comments and suggestions.

REFERENCES

[1] J. M. Chen and T. A. Black, "Defining leaf area index for non-flat leaves," *Plant, Cell Environ.*, vol. 15, no. 4, pp. 421–429, May 1992.

[2] G. Asrar, E. T. Kanemasu, R. D. Jackson, and P. J. Pinter, "Estimation of total above-ground phytomass production using remotely sensed data," *Remote Sens. Environ.*, vol. 17, no. 3, pp. 211–220, Jun. 1985.

[3] J. M. Chen, P. M. Rich, S. T. Gower, J. M. Norman, and S. Plummer, "Leaf area index of boreal forests: Theory, techniques, and measurements," *J. Geophys. Res., Atmos.*, vol. 102, no. D24, pp. 29429–29443, Dec. 1997.

[4] M. Khalili, M. R. Naghavi, A. P. Aboughadareh, and H. N. Rad, "Evaluation of relationships among grain yield and related traits in maize (Zea mays L.) cultivars under drought stress," *Int. J. Agronomy Plant Prod.*, vol. 4, no. 6, pp. 1251–1255, 2013.

[5] L. Wang, P. Wang, S. Liang, X. Qi, L. Li, and L. Xu, "Monitoring maize growth conditions by training a BP neural network with remotely sensed vegetation temperature condition index and leaf area index," *Comput. Electron. Agricult.*, vol. 160, pp. 82–90, May 2019.

[6] R. Žydelis, L. Weihermüller, M. Herbst, A. Klosterhalfen, and S. Lazauskas, "A model study on the effect of water and cold stress on maize development under nemoral climate," *Agricult. Forest Meteorol.*, vol. 263, pp. 169–179, Dec. 2018.

[7] R. Mangani, E. Tesfamariam, G. Bellocchi, and A. Hassen, "Growth, development, leaf gaseous exchange, and grain yield response of maize cultivars to drought and flooding stress," *Sustainability*, vol. 10, no. 10, p. 3492, 2018.

[8] R. Sandhu and S. Irmak, "Performance of AquaCrop model in simulating maize growth, yield, and evapotranspiration under rainfed, limited and full irrigation," *Agricult. Water Manage.*, vol. 223, Aug. 2019, Art. no. 105687.

[9] G. Nádor, D. Fényes, L. Vasas, and G. Surek, "Monitoring of maize damage caused by western corn rootworm by remote sensing," in *Proc. 28th Remote Sens. Changing Eur.*, Istanbul, Turkey, Jun. 2008, p. 255.

[10] S. Liu, J. Yang, C. F. Drury, H. Liu, and W. Reynolds, "Simulating maize (Zea mays L.) growth and yield, soil nitrogen concentration, and soil water content for a long-term cropping experiment in Ontario, Canada," *Can. J. Soil Sci.*, vol. 94, no. 3, pp. 435–452, 2014.

[11] X. Jin, L. Kumar, Z. Li, H. Feng, X. Xu, G. Yang, and J. Wang, "A review of data assimilation of remote sensing and crop models," *Eur. J. Agronomy*, vol. 92, pp. 141–152, Jan. 2018.

[12] H. Fang, S. Liang, and G. Hoogenboom, "Integration of MODIS LAI and vegetation index products with the CSM–CERES–Maize model for corn yield estimation," *Int. J. Remote Sens.*, vol. 32, no. 4, pp. 1039–1065, Feb. 2011.

[13] S. Karimi, A. A. Sadraddini, A. H. Nazemi, T. Xu, and A. F. Fard, "Generalizability of gene expression programming and random forest methodologies in estimating cropland and grassland leaf area index," *Comput. Electron. Agricult.*, vol. 144, pp. 232–240, Jan. 2018.

[14] E. Bériaux, F. Waldner, F. Collienne, P. Bogaert, and P. Defourny, "Maize leaf area index retrieval from synthetic quad pol SAR time series using the water cloud model," *Remote Sens.*, vol. 7, no. 12, pp. 16204–16225, 2015.

[15] C. Wang, S. Nie, X. Xi, S. Luo, and X. Sun, "Estimating the biomass of maize with hyperspectral and LiDAR data," *Remote Sens.*, vol. 9, no. 1, p. 11, 2017.

[16] H. Jin, A. Li, J. Wang, and Y. Bo, "Improvement of spatially and temporally continuous crop leaf area index by integration of CERES-maize model and MODIS data," *Eur. J. Agronomy*, vol. 78, pp. 1–12, Aug. 2016.

[17] L. Tao, J. Li, J. Jiang, and X. Chen, "Leaf area index inversion of winter wheat using modified water-cloud model," *IEEE Geosci. Remote Sens. Lett.*, vol. 13, no. 6, pp. 816–820, Jun. 2016.

[18] X. Jin, G. Yang, X. Xu, H. Yang, H. Feng, Z. Li, J. Shen, Y. Lan, and C. Zhao, "Combined multi-temporal optical and radar parameters for estimating LAI and biomass in winter wheat using HJ and RADARSAR-2 data," *Remote Sens.*, vol. 7, no. 10, pp. 13251–13272, 2015.

[19] C. Wang, J. Wu, and Y. Zhang, "Biophysical estimation of paddy rice with canopy scattering model and ALOS/PALSAR imagery in Southeast China," in *Proc. IEEE Int. Geosci. Remote Sens. Symp. (IGARSS)*, 2008, vol. 4, pp. IV-1185–IV-1188.

[20] C. Wang, J. Wu, Y. Zhang, G. Pan, J. Qi, and W. A. Salas, "Characterizing L-band scattering of paddy rice in Southeast China with radiative transfer model and multitemporal ALOS/PALSAR imagery," *IEEE Trans. Geosci. Remote Sens.*, vol. 47, no. 4, pp. 988–998, Apr. 2009.

[21] C. Jinsong, H. Yu, and D. Xinping, "Monitoring rice growth in Southern China using TerraSAR-X dual polarization data," in *Proc. 6th Int. Conf. Agro-Geoinf.*, Aug. 2017, pp. 1–4.

[22] B. N. Holben, C. J. Tucker, and C.-J. Fan, "Spectral assessment of soybean leaf area and leaf biomass," *Photogramm. Eng. Remote Sens.*, vol. 46, no. 5, pp. 651–656, 1980.

[23] A. Kross, H. McNairn, D. Lapen, M. Sunohara, and C. Champagne, "Assessment of RapidEye vegetation indices for estimation of leaf area index and biomass in corn and soybean crops," *Int. J. Appl. Earth Observ. Geoinf.*, vol. 34, pp. 235–248, Feb. 2015.

[24] A. Viña, A. A. Gitelson, A. L. Nguy-Robertson, and Y. Peng, "Comparison of different vegetation indices for the remote assessment of green leaf area index of crops," *Remote Sens. Environ.*, vol. 115, no. 12, pp. 3468–3478, Dec. 2011.

[25] A. Nguy-Robertson, A. Gitelson, Y. Peng, A. Viña, T. Arkebauer, and D. Rundquist, "Green leaf area index estimation in maize and soybean: Combining vegetation indices to achieve maximal sensitivity," *Agronomy J.*, vol. 104, no. 5, pp. 1336–1347, Sep. 2012.

[26] P. Curran, "Multispectral remote sensing for the estimation of green leaf area index," *Phil. Trans. Roy. Soc. London A, Math. Phys. Sci.*, vol. 309, no. 1508, pp. 257–270, 1983.

[27] T. Nicolas, V. Philippe, and W.-J. Huang, "New index for crop canopy fresh biomass estimation," *Spectrosc. Spectral Anal.*, vol. 30, no. 2, pp. 512–517, 2010.

[28] J. Wang, X. Xiao, R. Bajgain, P. Starks, J. Steiner, R. B. Doughty, and Q. Chang, "Estimating leaf area index and aboveground biomass of grazing pastures using Sentinel-1, Sentinel-2 and LandSAT images," *ISPRS J. Photogram. Remote Sens.*, vol. 154, pp. 189–201, Aug. 2019.

[29] M. A. Wulder, S. E. Franklin, and M. B. Lavigne, "High spatial resolution optical image texture for improved estimation of forest stand leaf area index," *Can. J. Remote Sens.*, vol. 22, no. 4, pp. 441–449, Dec. 1996.

[30] S. E. Franklin, M. A. Wulder, and M. B. Lavigne, "Automated derivation of geographic window sizes for use in remote sensing digital image texture analysis," *Comput. Geosci.*, vol. 22, no. 6, pp. 665–673, Jul. 1996.

[31] G.-H. Kwak and N.-W. Park, "Impact of texture information on crop classification with machine learning and UAV images," *Appl. Sci.*, vol. 9, no. 4, p. 643, 2019.

[32] M. A. Wulder, E. F. LeDrew, S. E. Franklin, and M. B. Lavigne, "Aerial image texture information in the estimation of northern deciduous and mixed wood forest leaf area index (LAI)," *Remote Sens. Environ.*, vol. 64, no. 1, pp. 64–76, Apr. 1998.

[33] M. E. Jakubauskas, "Effects of forest succession on texture in LandSAT thematic mapper imagery," *Can. J. Remote Sens.*, vol. 23, no. 3, pp. 257–263, Sep. 1997.

[34] M. Wulder, S. Franklin, and M. Lavigne, "Statistical texture properties of forest structure for improved LAI estimates from CASI," in *Proc. 26th Int. Symp. Remote Sens. Environ./18th Annu. Symp. Can. Remote Sens. Soc.*, Vancouver, BC, Canada, Mar. 1996, pp. 161–164.

[35] J. Zhou, R. Yan Guo, M. Sun, T. T. Di, S. Wang, J. Zhai, and Z. Zhao, "The effects of GLCM parameters on LAI estimation using texture values from quickbird satellite imagery," *Sci. Rep.*, vol. 7, no. 1, p. 7366, Dec. 2017.

[36] J. Yue, G. Yang, Q. Tian, H. Feng, K. Xu, and C. Zhou, "Estimate of winter-wheat above-ground biomass based on UAV ultrahigh-ground-resolution image textures and vegetation indices," *ISPRS J. Photogram. Remote Sens.*, vol. 150, pp. 226–244, Apr. 2019.

[37] Y. O. Ouma, "Optimization of second-order grey-level texture in high-resolution imagery for statistical estimation of above-ground biomass," *J. Environ. Informat.*, vol. 8, no. 2, pp. 70–85, Dec. 2006.

[38] J.-F. Bastin, N. Barbier, P. Couteron, B. Adams, A. Shapiro, J. Bogaert, and C. De Cannière, "Aboveground biomass mapping of African forest mosaics using canopy texture analysis: Toward a regional approach," *Ecol. Appl.*, vol. 24, no. 8, pp. 1984–2001, Dec. 2014.

[39] R. Pu and J. Cheng, "Mapping forest leaf area index using reflectance and textural information derived from WorldView-2 imagery in a mixed natural forest area in Florida, US," *Int. J. Appl. Earth Observ. Geoinf.*, vol. 42, pp. 11–23, Oct. 2015.

[40] S. T. Hlatshwayo, O. Mutanga, R. T. Lottering, Z. Kiala, and R. Ismail, "Mapping forest aboveground biomass in the reforested Buffelsdraai landfill site using texture combinations computed from SPOT-6 pan-sharpened imagery," *Int. J. Appl. Earth Observ. Geoinf.*, vol. 74, pp. 65–77, Feb. 2019.

[41] A. B. Debastiani, C. R. Sanquetta, A. P. D. Corte, N. S. Pinto, and F. E. Rex, "Evaluating SAR-optical sensor fusion for aboveground biomass estimation in a Brazilian tropical forest," *Ann. Forest Res.*, vol. 0, no. 0, 2019.

[42] H. Bach, M. Friese, K. Spannraft, S. Migdall, S. Dotzler, T. Hank, T. Frank, and W. Mauser, "Integrative use of multitemporal rapideye and TerraSAR-X data for agricultural monitoring," in *Proc. IEEE Int. Geosci. Remote Sens. Symp.*, Jul. 2012, pp. 3748–3751.

[43] M. Hosseini, H. McNairn, S. Mitchell, L. Dingle Robertson, A. Davidson, and S. Homayouni, "Synthetic aperture radar and optical satellite data for estimating the biomass of corn," *Int. J. Appl. Earth Observ. Geoinf.*, vol. 83, Nov. 2019, Art. no. 101933.

[44] L. Naidoo, H. van Deventer, A. Ramoelo, R. Mathieu, B. Nondlazi, and R. Gangat, "Estimating above ground biomass as an indicator of carbon storage in vegetated wetlands of the grassland biome of South Africa," *Int. J. Appl. Earth Observ. Geoinf.*, vol. 78, pp. 118–129, Jun. 2019.

[45] S. Gao, Z. Niu, N. Huang, and X. Hou, "Estimating the leaf area index, height and biomass of maize using HJ-1 and RADARSAT-2," *Int. J. Appl. Earth Observ. Geoinf.*, vol. 24, pp. 1–8, Oct. 2013.

[46] L. Xu, H. Zhang, C. Wang, B. Zhang, and M. Liu, "Crop classification based on temporal information using Sentinel-1 SAR time-series data," *Remote Sens.*, vol. 11, no. 1, p. 53, 2018.

[47] J. Clevers, L. Kooistra, and M. van den Brande, "Using Sentinel-2 data for retrieving LAI and leaf and canopy chlorophyll content of a potato crop," *Remote Sens.*, vol. 9, no. 5, p. 405, 2017.

[48] G. D. De Grandi, R. M. Lucas, and J. Kropacek, "Analysis by wavelet frames of spatial statistics in SAR data for characterizing structural properties of forests," *IEEE Trans. Geosci. Remote Sens.*, vol. 47, no. 2, pp. 494–507, Feb. 2009.
[49] M. E. J. Cutler, D. S. Boyd, G. M. Foody, and A. Vetrivel, "Estimating tropical forest biomass with a combination of SAR image texture and LandSAT TM data: An assessment of predictions between regions," *ISPRS J. Photogram. Remote Sens.*, vol. 70, pp. 66–77, Jun. 2012.
[50] R. M. Haralick, K. Shanmugam, and I. Dinstein, "Textural features for image classification," *IEEE Trans. Syst., Man, Cybern.*, vol. SMC-3, no. 6, pp. 610–621, Nov. 1973.
[51] R. M. Haralick, "Statistical and structural approaches to texture," *Proc. IEEE*, vol. 67, no. 5, pp. 786–804, May 1979.
[52] P. Kumar, R. Prasad, D. K. Gupta, V. N. Mishra, A. K. Vishwakarma, V. P. Yadav, R. Bala, A. Choudhary, and R. Avtar, "Estimation of winter wheat crop growth parameters using time series sentinel-1A SAR data," *Geocarto Int.*, vol. 33, no. 9, pp. 942–956, Sep. 2018.
[53] J. Rouse, R. Haas, J. Schell, and D. Deering, "Monitoring vegetationsystems in the great plains with erts," *NASA Special Publication*, vol. 351, p. 309, 1974.
[54] C. F. Jordan, "Derivation of leaf-area index from quality of light on the forest floor," *Ecology*, vol. 50, no. 4, pp. 663–666, Jul. 1969.
[55] G. Rondeaux, M. Steven, and F. Baret, "Optimization of soil-adjusted vegetation indices," *Remote Sens. Environ.*, vol. 55, no. 2, pp. 95–107, Feb. 1996.
[56] A. R. Huete, "A soil-adjusted vegetation index (SAVI)," *Remote Sens. Environ.*, vol. 25, no. 3, pp. 295–309, Aug. 1988.
[57] J. Qi, A. Chehbouni, A. R. Huete, Y. H. Kerr, and S. Sorooshian, "A modified soil adjusted vegetation index," *Remote Sens. Environ.*, vol. 48, no. 2, pp. 119–126, May 1994.
[58] H. Çamdevýren, N. Demýr, A. Kanik, and S. Keskýn, "Use of principal component scores in multiple linear regression models for prediction of chlorophyll—A in reservoirs," *Ecol. Model.*, vol. 181, no. 4, pp. 581–589, Feb. 2005.
[59] K. Stephan, C. A. Hibbitts, H. Hoffmann, and R. Jaumann, "Reduction of instrument-dependent noise in hyperspectral image data using the principal component analysis: Applications to Galileo NIMS data," *Planet. Space Sci.*, vol. 56, nos. 3–4, pp. 406–419, Mar. 2008.
[60] Y. Fei, S. Jiulin, F. Hongliang, Y. Zuofang, Z. Jiahua, Z. Yunqiang, S. Kaishan, W. Zongming, and H. Maogui, "Comparison of different methods for corn LAI estimation over northeastern China," *Int. J. Appl. Earth Observ. Geoinf.*, vol. 18, pp. 462–471, Aug. 2012.
[61] L. Wang, Q. Chang, J. Yang, X. Zhang, and F. Li, "Estimation of paddy rice leaf area index using machine learning methods based on hyperspectral data from multi-year experiments," *PLoS ONE*, vol. 13, no. 12, 2018, Art. no. e0207624.
[62] M. Stone, "Cross-validatory choice and assessment of statistical predictions (with discussion)," *J. Roy. Stat. Soc., B Methodol.*, vol. 38, no. 1, p. 102, Sep. 1974.
[63] X. Li, Y. Zhang, J. Luo, X. Jin, Y. Xu, and W. Yang, "Quantification winter wheat LAI with HJ-1CCD image features over multiple growing seasons," *Int. J. Appl. Earth Observ. Geoinf.*, vol. 44, pp. 104–112, Feb. 2016.

PEILEI LUO received the B.S. degree in remote-sensing science and technology from Shandong Agricultural University, Shandong, China, in 2014, and the M.S. degree in forestry information engineering from Beijing Forestry University, Beijing, China, in 2017. She is currently pursuing the Ph.D. degree in cartography and geographical information system with the Aerospace Information Research Institute, Chinese Academy of Sciences, Beijing.

Her research interests include crop growth parameter inversion and the integration of optical and microwave remote-sensing observations of maize.

JINGJUAN LIAO received the B.S. and M.S. degrees in geoscience from Nanjing University, Jiangsu, China, in 1987 and 1990, respectively, and the Ph.D. degree in geophysics from the Institute of Geophysics, Chinese Academy of Sciences, Beijing, China, in 1993.

Since 1993, she has been working on radar remote-sensing applications as a Researcher with the Institute of Remote Sensing Applications, Chinese Academy of Sciences. Since 2007, she has been working on microwave remote-sensing application as a Professor with the Center for Earth Observation and Digital Earth and the Institute of Remote Sensing and Digital Earth, Chinese Academy of Sciences. She currently works at the Key Laboratory of Digital Earth Science, Aerospace Information Research Institute, Chinese Academy of Sciences. She has completed several research projects. She has wide-ranging interests in remote-sensing applications for vegetation discrimination and classification, biomass estimation, and related radar backscattering modeling. She has published more than 50 articles in relevant journals. Her current research interests include remote sensing for estimating surface parameters and integration of remote-sensing observations of maize and mangrove.

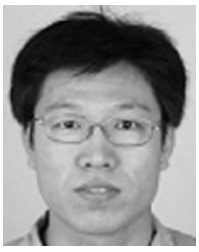

GUOZHUANG SHEN received the B.S. degree from Zhejiang University, in 2003, and the Ph.D. degree from the Institute of Remote Sensing Applications, Chinese Academy of Sciences, Beijing, China, in 2008.

Since 2008, he has been working at the Institute of Remote Sensing and Digital Earth, Chinese Academy of Sciences. He currently works at the Key Laboratory of Digital Earth Science, Aerospace Information Research Institute, Chinese Academy of Sciences. He mainly conducts research on flooding, variations in lakes due to global climate changes, and wetland ecosystems.